ACS APPLIED MATERIALS & INTERFACES

Research Article

www.acsami.org

Lightweight, Multifunctional Polyetherimide/Graphene@Fe_3O_4 Composite Foams for Shielding of Electromagnetic Pollution

Bin Shen, Wentao Zhai,* Mimi Tao, Jianqiang Ling, and Wenge Zheng*

Ningbo Key Lab of Polymer Materials, Ningbo Institute of Material Technology and Engineering, Chinese Academy of Sciences, Ningbo, Zhejiang Province 315201, China

Supporting Information

ABSTRACT: Novel high-performance polyetherimide (PEI)/graphene@Fe_3O_4 (G@Fe_3O_4) composite foams with flexible character and low density of about 0.28−0.4 g/cm^3 have been developed by using a phase separation method. The obtained PEI/G@Fe_3O_4 foam with G@Fe_3O_4 loading of 10 wt % exhibited excellent specific EMI shielding effectiveness (EMI SE) of ~41.5 dB/(g/cm^3) at 8−12 GHz. Moreover, most the applied microwave was verified to be absorbed rather than being reflected back, resulting from the improved impedance matching, electromagnetic wave attenuation, as well as multiple reflections. Meanwhile, the resulting foams also possessed a superparamagnetic behavior and low thermal conductiviy of 0.042−0.071 W/(m K). This technique is fast, highly reproducible, and scalable, which may facilitate the commercialization of such composite foams and generalize the use of them as EMI shielding materials in the fields of spacecraft and aircraft.

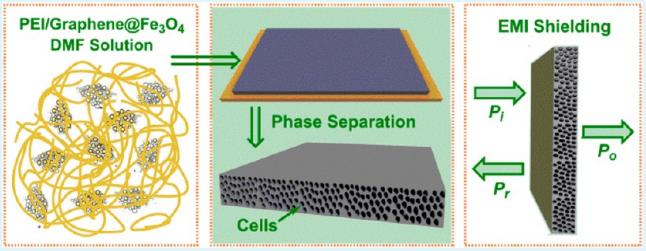

KEYWORDS: *polyetherimide, graphene@Fe_3O_4, foams, EMI shielding, superparamagnetic*

1. INTRODUCTION

In recent years, the increasing usage of electromagnetic wave devices, such as wireless networks, communication equipment, and personal digital devices, results in serious electromagnetic interference (EMI) problems in both military and civil applications.[1−4] Therefore, the rapid development of novel and high-performance EMI shielding materials has received considerable attention.[5,6] Polymer composites, which contains electrically conductive nanofillers, are becoming more attractive relative to the traditional metal-based EMI shielding materials because of their light weight, good processability, and resistance to corrosion. To further decrease the density of these conductive polymer composites on the basis of material and energy savings, researchers prefer the introduction of foam structures.[7−10]

Graphene, a newly discovered 2D carbon nanomaterial, not only possesses a stable structure but also exhibits high specific surface area and excellent electronic conductivity.[11−14] These properties make graphene very promising to provide remarkable EMI shielding in polymer composite foams.[15,16] Moreover, researchers have grown different inorganic nanocrystals on the surface of graphene,[17−21] yielding nanocrystal-functionalized graphene possessing not only the individual property of graphene and nanocrystals, but also additional function derived from the synergy between them.[22−26] As such, they have been widely used in the areas of supercapacitors, electrochemical analysis, catalysts, lithium batteries, and many others. Inspired by this understanding, we propose that the introduction of such nanocrystal-functionalized graphene into polymer foams would endow the composite foams with excellent EMI shielding property, as well as some additional properties due to the presence of nanocrystals.

Magnetic nanoparticles (NPs), which have many applications in environmental, electronic, and biological process,[27−29] are one of such nanocrystals because of their excellent magnetic properties. Among them, Fe_3O_4 NPs have been focused on greatly because of their good biocompatibility and low toxicity. The functionalization of graphene with Fe_3O_4 NPs could contribute the high complex permeability values to graphene because of their large saturation magnetization,[30] and thus improve the electromagnetic wave absorption property.[31−33] In addition, magnetic Fe_3O_4 NPs could avoid the skin effect that easily happens in the case of high conductive nanofiller and make the electromagnetic waves enter effectively due to their high resistivity.[32] As a result, the introduction of Fe_3O_4-functionalized graphene (graphene@Fe_3O_4) into polymer composite foams would result in strong electromagnetic wave absorption. Meanwhile, an attractive functionality that can be readily induced to polymer composite foams by the introduction of graphene@Fe_3O_4 (G@Fe_3O_4), is superparamagnetism. The resulting foams should have the polymer flexibility and could be actuated by using an magnetic field. Furthermore, the existence of Fe_3O_4 NPs on graphene could prevent the aggregation of graphene sheets, and the presence of graphene sheets can also inhibit the intrinsical aggregation of magnetic particles.[29,34] Therefore, G@Fe_3O_4 is an ideal

Received: August 28, 2013
Accepted: October 17, 2013
Published: October 17, 2013

candidate to prepare multifunctional polymer composite foams for excellent EMI shielding.

Polyetherimide (PEI), one kind of high-performance polymer, possesses a high glass transition temperature (T_g) of 215 °C, low smoke generation, desirable flame retardancy, and excellent mechanical properties. Thus, the selection of PEI as the polymer matrix to prepare high-performance graphene-based polymer composite foams for EMI shielding is very valuable. However, it is a challenge to fabricate the satisfied PEI foams using the physical blowing agent, especially at high filler loading, possibly because of its extremely long saturation time (280−520 h) and low expansion ratio (<2 times).[35−37] To solve this technical problem, our group has explored a facile but effective approach for massively fabricating lightweight PEI composite foam with high nanofiller loading based on a water-vapor induced phase separation (WVIPS) process.[38]

Here, in the present work, novel high-performance PEI/G@Fe_3O_4 composite foams with excellent EMI shielding effciency and low density of 0.28−0.40 g/cm^3 have been developed using a WVIPS method (Figure 1). The presence of Fe_3O_4 improved

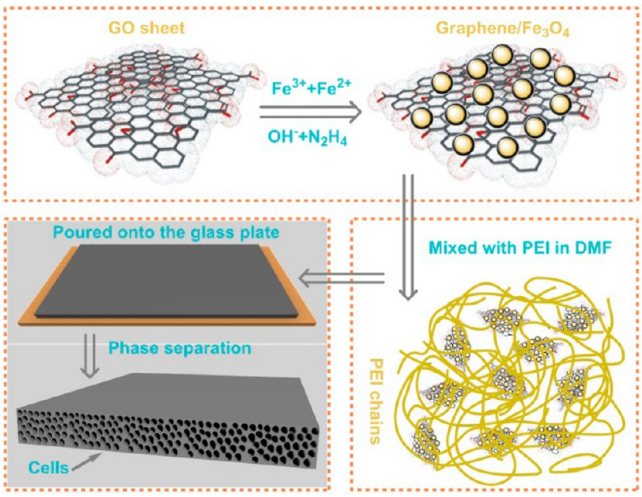

Figure 1. Schematic of the preparation of G@Fe_3O_4 hybrid and PEI/G@Fe_3O_4 composite foams by a WVIPS process.

the electromagnetic wave absorption of PEI foams and endowed the material with the superparamagnetism. Meanwhile, the thermal conductivity of these foams was not significantly increased though the presence of graphene with superior thermal conductivity, indicating an excellent thermal insulation performance. This technique is fast, highly reproducible, and scalable, which may facilitate the commercialization of such composite foams and generalize the use of them as EMI shielding materials in the fields of spacecraft and aircraft.

2. EXPERIMENTAL SECTION

Materials. Graphite oxide (GO) was synthesized by the Staudenmaier's method from pristine graphite flakes (35 μm) as reported in our previous work.[39−41] Ferrous chloride tetrahydrate ($FeCl_2.4H_2O$) and ferric chloride hexahydrate ($FeCl_3.6H_2O$) were obtained from Aladdin Reagent Co., Ltd. PEI resins (Ultem1000) having a density of 1.28 g/cm^3 and T_g of 215 °C were purchased from GE Company. All other reagents were used as received from Sinopharm Chemical Reagent (China).

Synthesis of G@Fe_3O_4 Hybrid. The brown GO suspension (1 mg/mL) was obtained by exfoliating 100 mg of GO flakes in 100 mL of distilled water with the assistance of sonication (300 W, 20 Hz). To prepare the G@Fe_3O_4 hybrid, we dropwise added the solutions of $FeCl_2{\cdot}4H_2O$ (0.1 g in 5 mL water) and $FeCl_3{\cdot}6H_2O$ (0.25 g in 10 mL water) into the as-prepared GO suspension under continuous stirring in nitrogen atmosphere. After 10 min, ammonium hydroxide ($NH_3{\cdot}H_2O$) solution (16 mL) was dropwise added into the mixture for 10 min. The mixture was then further reduced by hydrazine (a reducing agent) at 90 °C for 6 h. After being cooled to room temperature, the black precipitate in the solution was collected by removing the supernatant and washing with distilled water several times. Finally, the wet precipitate was freeze-dried for 24 h to obtain G@Fe_3O_4 hybrid.

Preparation of PEI/G@Fe_3O_4 Foams. The PEI/G@Fe_3O_4 composite foams was prepared by a WVIPS process as described in our previous work.[38] First, the DMF/G@Fe_3O_4 suspension was obtained by sonicating a certain amount of G@Fe_3O_4 powder in dimethylformamide (DMF) for 10 min. Then, the PEI pellets were completely dissolved in G@Fe_3O_4 suspension with vigorous stirring at 70 °C for 12 h. After that, the final suspension was kept still to remove air bubble and then poured onto a substrate (clean glass plate was used here) and exposed in ambient atmosphere with temperature of ∼22 °C and humidity of ∼75% for 4 h. Finally, the solidified composite foam sheets were immersed into 30 °C fresh water to remove the residual DMF, followed by drying at 150 °C for 24 h. For comparison, the PEI/Fe_3O_4 foam with 10.0 wt % loading was also prepared using the same procedure.

Characterizations. Transmission electron microscopy (TEM) images were obtained by using a TECNAI 20 with a operating voltage of 200 kV. To prepare G@Fe_3O_4 sample, the DMF/G@Fe_3O_4 dispersion, which was prepared by dispersing 5 mg of G@Fe_3O_4 in 25 mL of DMF under ultrasonication for 30 min, was dropped on an amorphous carbon-coated copper grid and then dried in air. To prepare the foam sample, a foam sheet embedded in epoxy resin was cryogenically cut into ultrathin sections by diamond knife using a microtome and collected on copper grids. X-ray diffraction (XRD) data were collected on a Bruker AXS X-ray diffractometer with CuKa radiation at a generator current of 40 mA and voltage of 40 kV. Raman spectra were recorded with Labram spectrometer (Super LabRam II system) with a laser of 633 nm. X-ray photoelectron spectroscopy (XPS) was performed with a Kratos AXIS ULTRA system using Al (mono) Kα radiation. The magnetization performance was measured by using a model-9 PPSM (Quantum Design). Scanning electron microscopy (SEM) images was obtained by using a Hitachi S-4800 field emission SEM at 4 kV. The EMI shielding performance was performed with a WILTRON 54169A scalar measurement system at room temperature in X-band (8−12 GHz). To fit the sample holders for the measurement, the foam samples with a thickness of 2.5 mm were cut to small pieces with the size of 22.5 × 10.0 mm^2. The thermal conductivity of the samples was determined by NETZSCH LFA 457 MicroFlash analysis system. In cases, at least five samples were tested from which the average value was calculated.

3. RESULTS AND DISCUSSION

Characterizations of G@Fe_3O_4 Hybrid. As we know, the solubility of pristine graphene in solvents is poor due to the absence of oxygen-contained functional groups. Therefore, GO is always used as a direct starting material to fabricate graphene-based hybrids, because it possesses abundant oxygen groups and can steadily suspended in water and organic solvents. Here, the G@Fe_3O_4 hybrid was prepared by chemical deposition of iron ions onto GO sheets and then chemical reduction of GO with hydrazine. The weight ratio between the GO and Fe_3O_4 was about 1:1. From the representative TEM image of G@Fe_3O_4 hybrid (Figure 2a), we can see that the surface of graphene has been homogenously covered by narrowly distributed Fe_3O_4 NPs with an average diameter of 11 nm (Figure 2b). It may be because that the oxygen groups on GO surface can act as the nucleation center, interacting with iron ions during the chemical deposition. The lattice fringe spacing

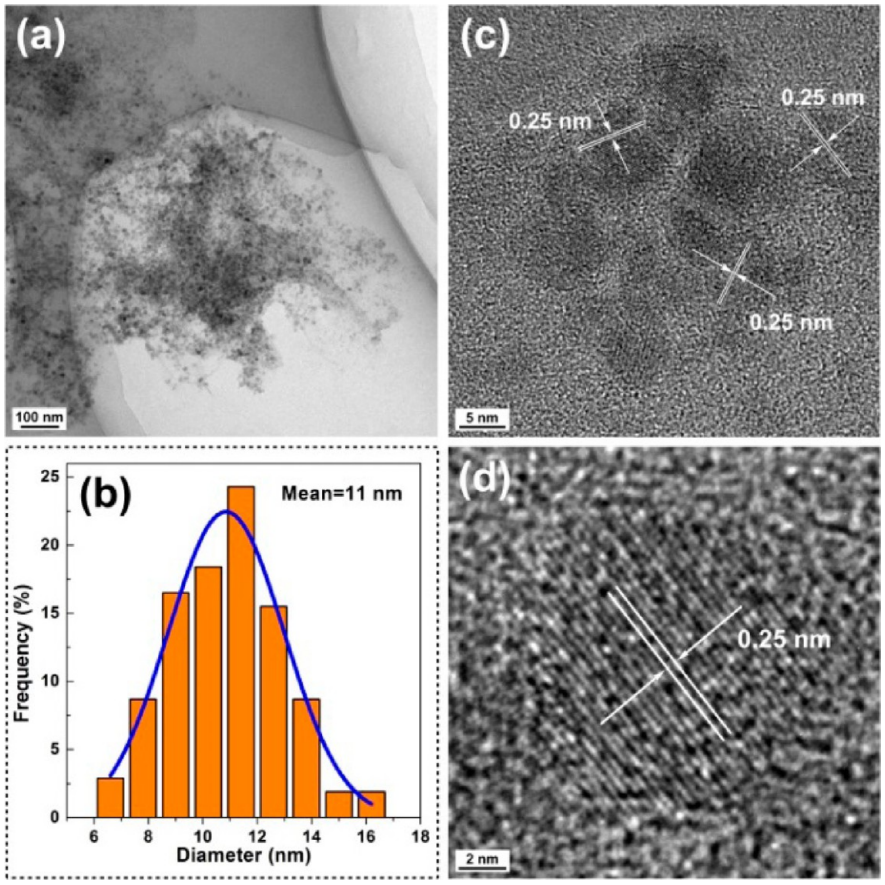

Figure 2. (a, b) TEM image of G@Fe_3O_4 with corresponding size distributions of Fe_3O_4 nanoparticles; (c, d) high-resolution TEM image of G@Fe_3O_4 shows the interplane of Fe_3O_4.

(0.25 nm) showed in the TEM image (Figure 2c, d) was well-consistent with the lattice spacing of cubic magnetite in (311) planes.

The crystalline structure of Fe_3O_4 NPs on graphene was characterized by XRD diffraction. As shown in Figure 3a, the characteristic diffraction peaks of Fe_3O_4NPs are present in the obtained G@Fe_3O_4 hybrid, which can be assigned to the (111), (220), (311), (400), (422), (511), (440), and (533) planes according to JCPDS 19−629 (JCPDS = Joint Committee on Powder Diffraction Standards). Raman spectroscopy was used to investigate the structural change during the reduction process of G@Fe_3O_4, and the results are shown in Figure 3b. Compared with pristine GO, the G-band of graphene in G@Fe_3O_4 red-shifted from 1596 to 1588 cm^{-1}, which was closed to that of pristine graphite (1579 cm^{-1}),[39] implying the successful reduction of GO or the attachment of Fe_3O_4 NPs on the reduced GO surface.[42,43] The intensity ratio of D-band and G-band (I(D/G)) is always related to the ratio of disordered sp^3 and ordered sp^2 carbon domains.[44] Here, the calculated I(D/G) of G@Fe_3O_4 increased from 1.08 to 1.45, suggesting the decrease in the average size of sp^2 carbon domains, which could be explained by the creation of more numerous but smaller sp^2 carbon domains after the reduction, as well as the presence of some unrepaired defects.[45,46]

The XPS spectrum was used to further analysis the chemical composition of G@Fe_3O_4. As shown in Figure 3c, the C 1s XPS spectrum of graphene in G@Fe_3O_4 can be deconvoluted into four carbon components with different binding energy: C−C/C═C (∼284.6 eV), localized alternant hydrocarbon (∼285.3 eV),[47,48] C−O−C/C−OH (∼286.5 eV), and carboxyl C═O/O−C═O (∼288.3 eV). Obviously, the intensity of oxygen groups in G@Fe_3O_4 has a noticeable decrease relative to that of GO (see Figure S1 in the Supporting Information), indicating the successful removal of oxygen groups during the chemical reduction. Furthermore, the percentage of each carbon component was calculated according to the ratios of peak areas. As displayed in Table S1 in the Supporting Information, the C−O−C/C−OH component of the hybrid decreased to 8.5 atom % as compared with that of GO (38.1 atom %), confirming the successful removal of oxygen groups and the formation of graphene structure in the hybrid after chemical reduction. Moreover, in the Fe2p XPS spectrum of G@Fe_3O_4, the binding energy peaks at 710.9 and 724.9 eV agreed well with that of $Fe2p_{3/2}$ and $Fe2p_{1/2}$, respectively.

Magnetic properties of G@Fe_3O_4 were investigated using a Model-9 PPSM (Quantum Design), as shown in Figure 3d. The magnetization curves were recorded at room temperature in the magnetic field range from −20 to 20 kOe. Compared with pure bulk Fe_3O_4, the magnetic saturation value (M_s) of G@Fe_3O_4 decreased from 75.9 to 14.0 emu/g. The reduced value might be ascribed to the nanoscale size of Fe_3O_4 NPs and the presence of graphene sheets.[23,49,50] The magnetization curves show reversible, nonlinear characteristic with no significant coercivity (∼45 Oe as shown in Figure S2 in the Supporting Information) after removing the applied magnetic field, implying that the G@Fe_3O_4 was superparamagnetic. Furthermore, our G@Fe_3O_4 hybrid could be easily separated under a magnet (insert in Figure 3d).

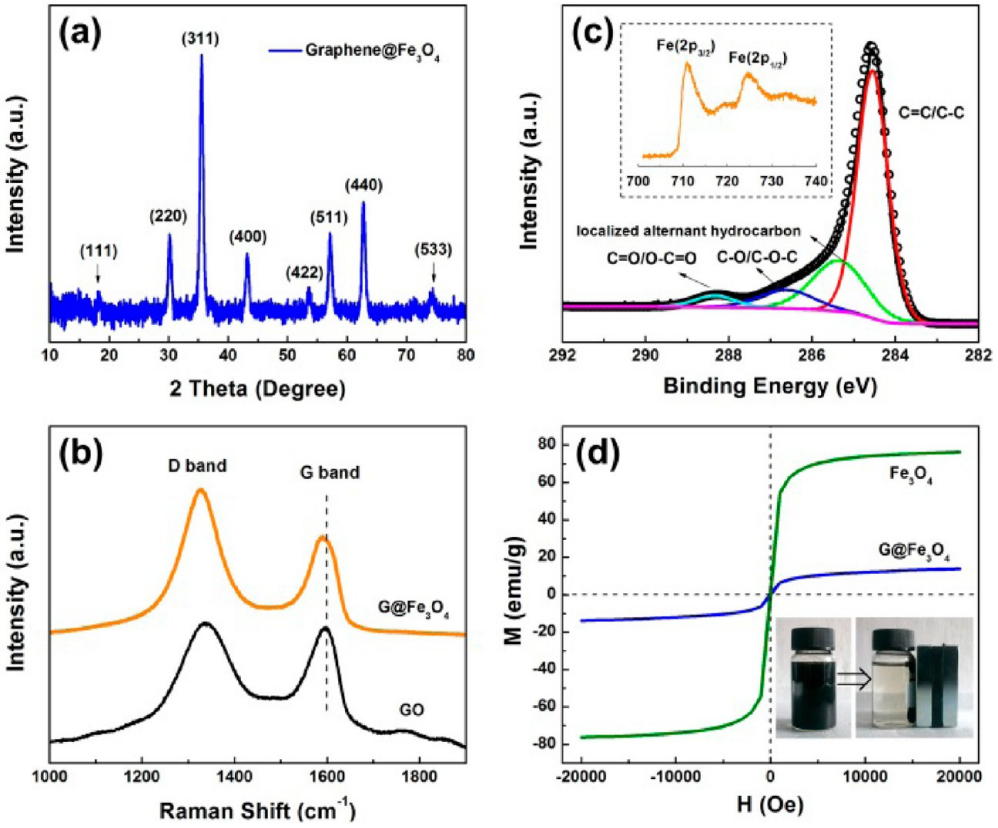

Figure 3. (a) XRD pattern of $G@Fe_3O_4$; (b) Raman spectra of GO and $G@Fe_3O_4$ with a laser of 633 nm; (c) XPS spectra of $G@Fe_3O_4$ and the inset shows Fe 2p spectra of $G@Fe_3O_4$; (d) magnetization hysteresis loops of $G@Fe_3O_4$ at room temperature. The bottom right inset shows the photographs of $G@Fe_3O_4$ in water and their response to an external magnetic field.

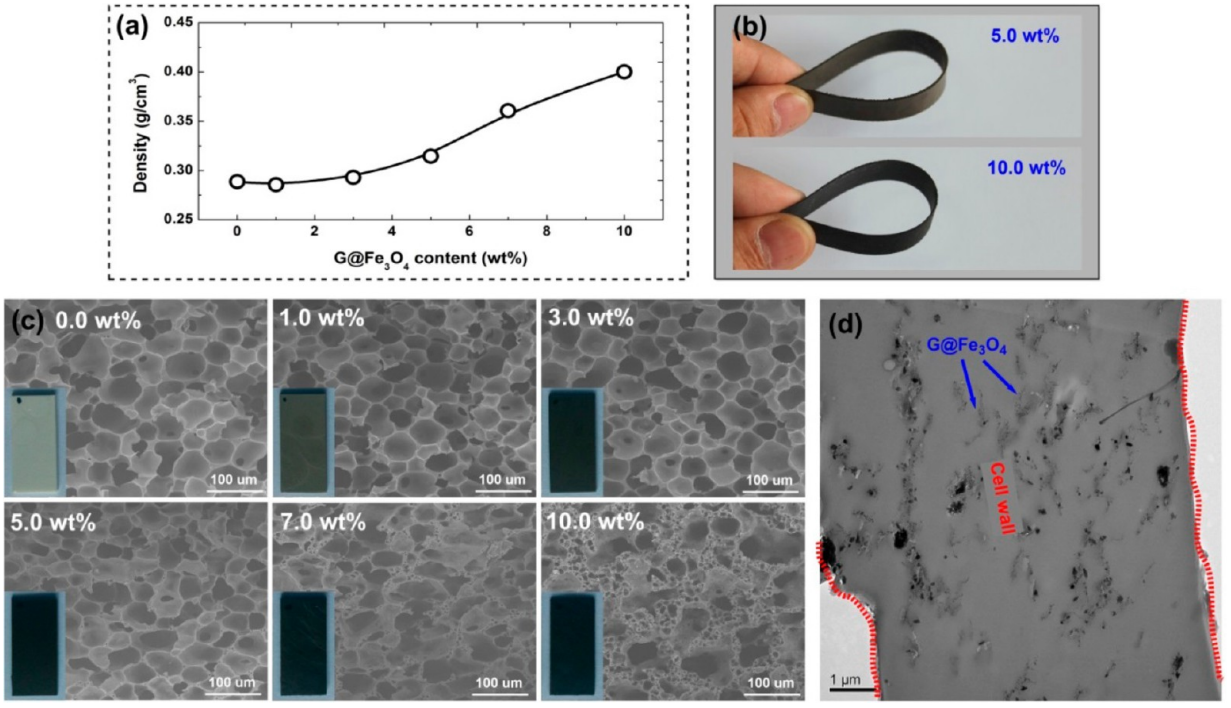

Figure 4. (a) Density of the PEI/$G@Fe_3O_4$ foams asthe function of $G@Fe_3O_4$loading; (b) optical photographs of the foam sheets under bending; (c) SEM images of the PEI/$G@Fe_3O_4$ foams with different $G@Fe_3O_4$ loading; (d) TEM image to show the dispersion of $G@Fe_3O_4$ sheets in cell wall of the foam with 5 wt % $G@Fe_3O_4$.

Microcellular PEI/$G@Fe_3O_4$ Foams. The microcellular PEI/$G@Fe_3O_4$ foams with different $G@Fe_3O_4$ loadings were synthesized according to the WVIPS technique. The densities of these foams were measured via the water displacement

method according to ASTM D792. As shown in Figure 4a, the density of PEI/G@Fe_3O_4 foam was about 0.28−0.40 g/cm^3 at 1.0−10.0 wt % loading, which is much lower than the density of PC/silica foam blown with the compressed CO_2 and with the similar nanofillers loading.[37] Figure 4b shows the typical optical photographs of the foams with G@Fe_3O_4 loading of 5.0 and 10.0 wt %. It was obvious that the obtained foam sheets were quite flexible under bending. The typical SEM images of the fracture surface of the foams were also shown in Figure 4c. It is clear that the uniform microcellular cell structures were formed in foams at lower G@Fe_3O_4 loading of 1−5 wt %. This unique structure is ascribed to the occurrence of phase separation due to the diffusion of water vapor into the composite solution. However, the increased G@Fe_3O_4 loading (7.0 and 10.0 wt %) induced the formation of the bimodal distributon of cell structures (small cells existed around the big cell), possibly because of the enhanced viscosity of suspension and the aggregration of G@Fe_3O_4 at higher contents.[51] To determine the dispersion of G@Fe_3O_4 sheets, we conducted further TEM observation on the ultrathin sections of the foam. The result is shown in Figure 4d. Obviously, the G@Fe_3O_4 sheets are well-dispersed and relatively aligned in the cell wall of the foam, and a large number of Fe_3O_4 NPs are located on both sides of graphene sheets.

Superparamagnetic Behavior and Magnetic Actuation. The magnetic performance of the PEI/G@Fe_3O_4 foams was investigated by monitoring their magnetization with an applied magnetic field ranging from −20 to 20 kOe at room temperature. For the sake of comparison, the magnetization was normalized based on the total weight of the composite foam (PEI + G@Fe_3O_4). As shown in Figure 5a, the M_s of the foams was in the range of 0.38−3.09 emu/g, and tended to linearly increase with the G@Fe_3O_4 content (inset at the lower right). Compared to the G@Fe_3O_4 hybrids, the magnetization of foams significantly decreased because of the reduced G@Fe_3O_4 concentration. Moreover, it is interesting to find that the obtained PEI/G@Fe_3O_4 foams were superparamagnetic since there was no significant hysteresis in the M_s (Figure 5a, inset at the top left). The coercivity of all these foams was in the range of 35 ± 5 Oe, which was close to the coercivity value of G@Fe_3O_4 hybrid. This phenomenon demonstrated that the G@Fe_3O_4 had retained their superparamagnetism after being compounding with polymer matrix. Therefore, our PEI/G@Fe_3O_4 microcellular foams could be actuated by a magnetic field. The magnetic response of PEI/G@Fe_3O_4 foam with 10 wt % loading in the absence ($B = 0$) and presence ($B > 0$) of a magnetic field is shown in Figure 5b (left) Clearly, Once a permanent magnet was approached, this microcellular foam cantilever was actuated with a fast response time. Similarly, this foam sheet also exhibited a strong attraction to a static magnetic field as shown in Figure 5b (right).

Electromagnetic Interference (EMI) Shielding. The EMI shielding effectiveness (EMI SE) is defined as the logarithmic ratio of incoming (P_i) to outgoing power (P_o) of radiation. In general, decibels (dB) is used to express the efficiency of the shielding material. In this study, the EMI SE of PEI/G@Fe_3O_4 foams with a thickness of 2.5 mm was measured in X-band (8−12 GHz). As shown in Figure 6a, the EMI SE of all the foams exhibited weak frequency dependency in the measured bands. The EMI SE of the foam with 1.0 wt % G@Fe_3O_4 is measured to be 3.5−5.8 dB over the frequency range of 8−12 GHz. However, when the G@Fe_3O_4 content increased to 5.0 wt %, the EMI SE value was found to vary from 6.5 to 9.2

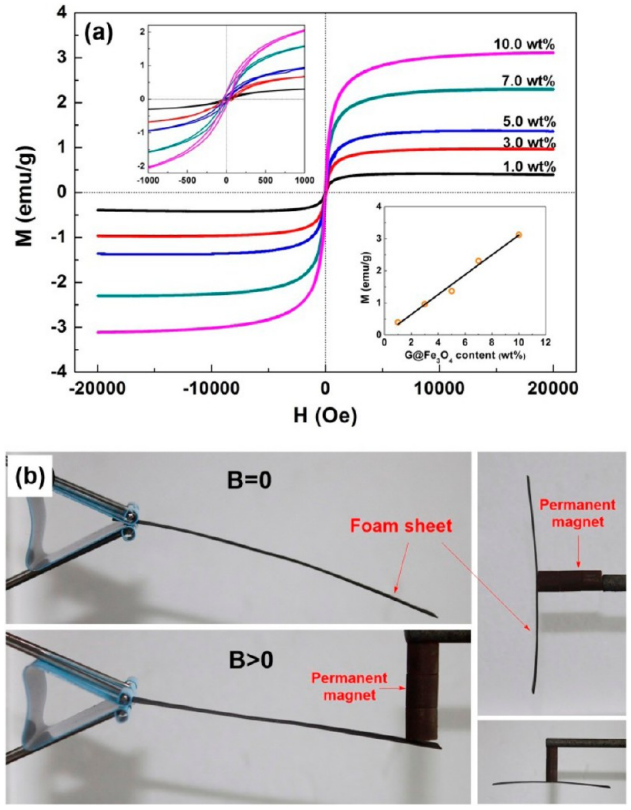

Figure 5. Superparamagnetic microcellular PEI/G@Fe_3O_4 foam sheets: (a) Magnetization of the composite foams with different G@Fe_3O_4 loading; (b) this free-standingcomposite foam sheet can be actuated by an external magnetic field.

dB. The EMI SE value increased up to 11.2−14.3 dB for the foam with 7.0 wt % G@Fe_3O_4 and to a much higher value (14.3−18.2 dB) for the foam with 10.0 wt % G@Fe_3O_4, which denotes that EM shielding properties of these foams are enhanced with the increase of G@Fe_3O_4 loading. As the EMI performance usually increases with increasing the material thickness,[52,53] we have reason to believe that the EMI SE value for our PEI foam can be improved to reach the target value (~20 dB) required for practical application by slightly increasing the thickness of specimen.

Generally, phenomena such as transmission, reflection, and absorption can be observed, when the microwave radiation is incident on a shielding material.[54] To further clarify the EMI shielding mechanism in PEI/G@Fe_3O_4 foams, the total EMI shielding effectiveness (SE_{total}), we calculated microwave reflection (SE_R) and microwave absorption (SE_A) at 9.6 GHz from the measured scattering parameters (S_{11} and S_{21}); the results are shown in Figure 6b. Clearly, the increase in G@Fe_3O_4 loading led to the enhancement of both SE_{total} and SE_A and the contribution of SE_R could be negligible for all of the microcellular foams with different G@Fe_3O_4 loadings. For example, the SE_{total}, SE_A, and SE_R were 13.1, 12.7, and 0.4 dB for the foam with 7.0 wt % G@Fe_3O_4, whereas the corresponding values were 17.8, 17.3, and 0.5 dB for the foam with 10.0 wt % G@Fe_3O_4, respectively. The results indicated that most of microwave power was dissipated as heat through the microcellular foams rather than being reflected back from the foams' surface, which confirmed that absorption was the main EMI shielding mechanism in the X-band frequency region for such microcellular foams.

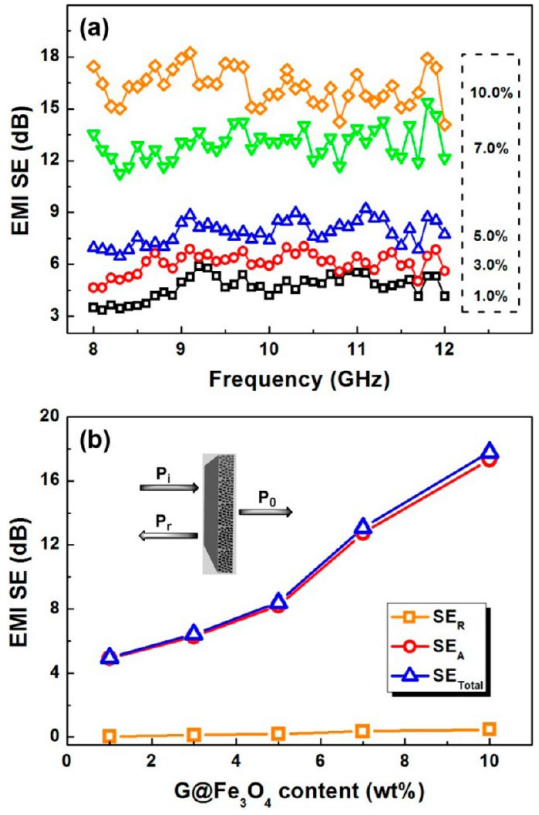

Figure 6. (a) EMI shielding effectiveness as a function of frequency measured in the 8−12 GHz range of the PEI/G@Fe_3O_4 foams with various G@Fe_3O_4 concentrations; (b) SE_{total}, SE_R, and SE_A of microcellular foams at 9.6 GHz;.

One factor that contributes to microwave absorption is impedance matching. As displayed in Figure S3 in the Supporting Information, the DC electrical conductivity of the PEI/G@Fe_3O_4 foams was lower than that of the PEI/graphene foams reported in our previous study.[38] This phenomenon suggested that the introduction of Fe_3O_4 NPs tended to decrease the electrical conductivity of the composite foams, which would improve the equality of the electromagnetic parameters, and thus improve the level of impedance matching and decrease the surface reflection.[32] Another important factor that contributes to microwave absorption is electromagnetic wave attenuation, determined by dielectric loss and magnetic loss.[31,32,55] As we know, electronic, ionic, orientational, and space charge polarization determines the total dielectric property of the material. In a heterogeneous system, the accumulation of virtual charges at the interface of two medium with different conductivities and dielectric constants would lead to interfacial polarization and is known as Maxwell−Wagner polarization. Pristine graphene is nonmagnetic and contributes to microwave absorption mostly due to its dielectric loss. The introduction of Fe_3O_4 NPs on graphene sheets would not only enhance the magnetic losses but also enhance the dielectric losses in a wide frequency range, resulting from the interfacial polarizations between the Fe_3O_4 NPs and graphene because of the formation of a heterogeneous system and more interfaces, as well as the stronger coupling at the gaps between the neighboring Fe_3O_4 NPs.[31] Furthermore, the presence of oxygen groups and defects on the reduced graphene could help to improve the microwave absorption of the composite foams.[32]

In addition, multiple reflections could be another adsorbing mechanism, which mainly results from the reflection at various interfaces or surfaces in the shielding material.[56] As indicated in Figure 7a, the microcells in the PEI/G@Fe_3O_4 foams provided a large cell-matrix interface area. The incident electromagnetic waves entering the composite foam could be repeatedly reflected and scattered between these interfaces, and they were hard to escape from the composite foam until being dissipated as heat.[16,38,56] Moreover, the layered structure and large aspect ratio of G@Fe_3O_4 hybrid may also cause the

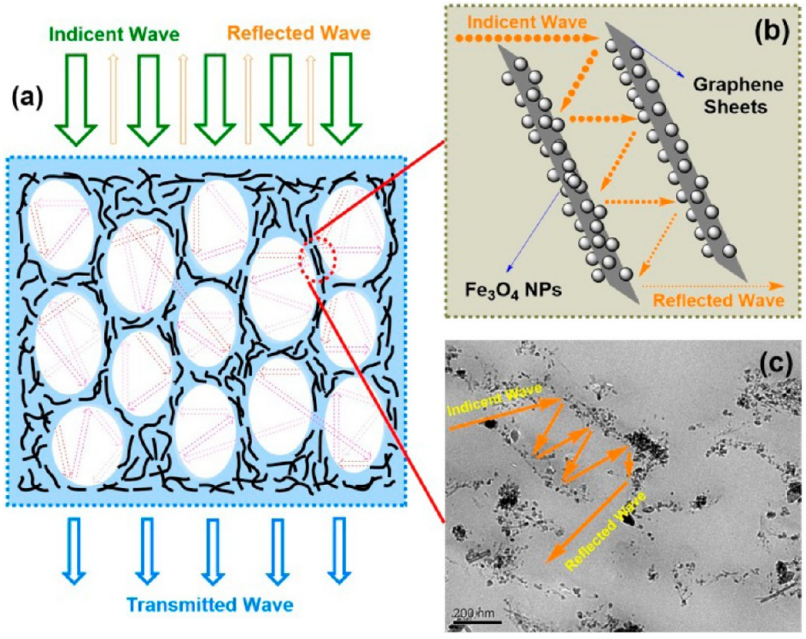

Figure 7. (a) Schematic description of electromagnetic wave transfer across the PEI/G@Fe_3O_4 foams; (b) schematic diagram representing the multireflection route of electromagnetic wave between the G@Fe_3O_4 sheets; (c) TEM image showing two parallelG@Fe_3O_4 sheets in the matrix as well as the possible reflection path of electromagnetic wave.

multiple reflection. As demonstrated in Figure 7b and Figure 7c, the two parallel G@Fe_3O_4 sheets may reflect and scatter the incident electromagnetic waves many times between the sheets inside, increasing their propagation paths in the composite foam, which could further enhance the absorbing ability. This phenomenon is much like the case in ordered mesoporous carbon/fused silica composites.[57] In brief, the multireflections of microwaves could lead to the additional losses of electromagnetic energy based on the microcells and G@Fe_3O_4 sheets.

As proposed by previous study,[7,8,38,43] the specific EMI SE (EMI SE divided by density) would be more suitable for comparing the shielding performance between typical metals and lightweight polymer composite foams for aircraft and spacecraft applications. As shown in Figure 8, the PEI/G@

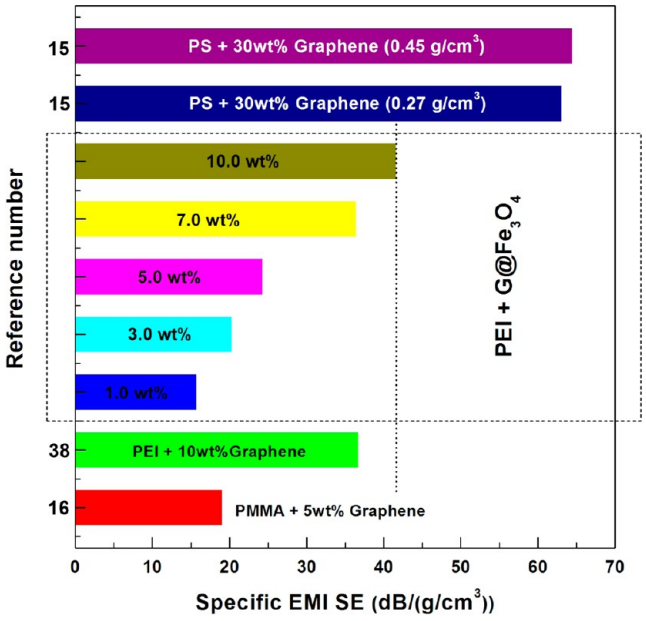

Figure 8. Comparison of specific EMI shielding effciency of our PEI/G@Fe_3O_4 foams with other reported results.

Fe_3O_4 foams exhibited the increased average specific EMI SE from 15.6 dB/(g/cm^3) to 41.5 dB/(g/cm^3) in the frequency range. It is worth noting that the shielding performance of our PEI foam with 10.0 wt % G@Fe_3O_4 were higher as compared to that of PMMA foam with 5.0 wt % graphene,[16] and PEI foam with 10.0 wt % graphene.[38] However, a higher specific EMI SE in porous polystyrene/graphene composites with poor cell structure has also been reported because of the higher filler loading of 30 wt %.[15] For comparison, the PEI/Fe_3O_4 foam (~0.40 g/cm^3) with 10.0 wt % loading was also prepared, and the specific EMI SE of this foam was calculated to be 15.2 dB/(g/cm^3), which was lower than that of PEI/G@Fe_3O_4 foam, possibly due to their high resistivity as well as their poor dispersion in the foam, resulting from the intrinsical aggregation of magnetic NPs. Furthermore, the contribution of SE_A to SE_{total} of our PEI foam containing 10.0 wt % G@Fe_3O_4 was 97.2%, which is much higher than that of PEI foam (90.6%) containing 10.0 wt % graphene.[38] As discussed above, this enhanced EMI shielding performance should be attributed to the presence of Fe_3O_4 NPs on graphene, as well as the synergy between them. These results strongly suggest that such microcellular PEI/G@Fe_3O_4 foams are very promising for use as lightweight and high-performance EMI shielding materials with strong microwave absorption.

Thermal Conduction Performance. The thermal insulation of EMI shielding materials is critical for aircraft and spacecraft to minimize the temperature impact on the working performance of electronic devices and people in it. Thus, the thermal conductivity of pristine PEI foam and the PEI/G@Fe_3O_4 foams was measured using a Laser Flash System. As shown in Figure 9, pristine PEI foam has a thermal conductivity

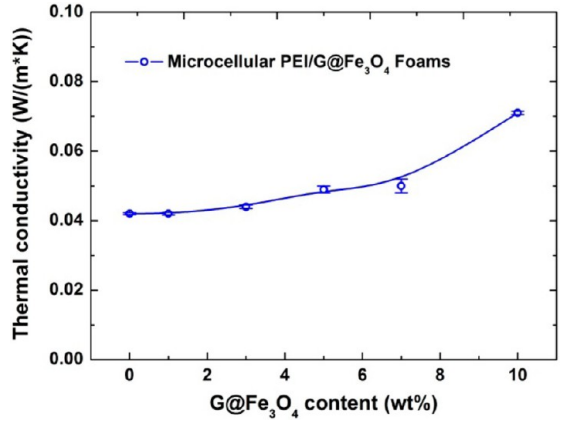

Figure 9. Thermal conductivity of microcellular PEI/G@Fe_3O_4 foams at room temperature.

of 0.042 W/(m K). The introduction of 10.0 wt % G@Fe_3O_4 only increased the thermal conductivity of the composite foam to 0.071 W/(m K). Generally, the thermal conductivity of the composite foam is affected by two factors: the change of cell size and the addition of nanofillers.[58−60] It has been well accepted that the decrease of average cell size would usually decrease the thermal conductivity. Conversely, the introduction of nanofillers with excellent thermal conductivity would significantly increase the thermal conductivity. In this work, the decreased cell size would reduce the thermal conductivity. The improved thermal conductivity in the composite foams should therefore be attributed to the excellent thermal conductivity of graphene sheets. Nevertheless, the increase in foam's thermal conductivity is very limited, which suggested that such loading of G@Fe_3O_4 would not hinder the thermal insulation performance of PEI/G@Fe_3O_4 foams.

4. CONCLUSIONS

In summary, we have developed a fast, highly reproducible, and scalable approach to prepare a new type of high-performance polymer composite foams with strong electromagnetic wave absorption by incorporating a hybrid structure of grahene@Fe_3O_4 into the PEI matrix and then foaming using a WVIPS method. The as-prepared foams possessed microcellular cell structure and their density was in the range of 0.28 to 0.40 g/cm^3. The EMI SE of these foams were enhanced with the increase of G@Fe_3O_4 content and the foam with 10.0 wt % loading displayed a high EMI SE of ~14.3−18.2 dB over a frequency range of 8−12 GHz. Because of the improved impedance matching and electromagnetic wave attenuation resulting from the introduction of Fe_3O_4, as well as the existence of multiple reflections, most of electromagnetic wave was adsorbed rather than being reflected back from the foams. Furthermore, the present foams are superparamagnetic and could be magnetically actuated. Meanwhile, the thermal

conductivity of these foams was measured to be 0.042−0.071 W/(m K), indicating an excellent thermal insulation performance.

■ ASSOCIATED CONTENT

Supporting Information

Providing the XPS analysis of GO and the electrical conductivity of PEI composite foams. This material is available free of charge via the Internet at http://pubs.acs.org/.

■ AUTHOR INFORMATION

Corresponding Authors

*Tel.: +86 0574 8668 5256. Fax: +86 0574 8668 5186. E-mail: wtzhai@nimte.ac.cn.

*E-mail: wgzheng@nimte.ac.cn.

Notes

The authors declare no competing financial interest.

■ ACKNOWLEDGMENTS

The authors are grateful to the National Natural Science Foundation of China (Grants 51003115), and Ningbo Key Lab of Polymer Materials (Grant 2010A22001) for their financial support of this study.

■ REFERENCES

(1) Ohkoshi, S.-i.; Kuroki, S.; Sakurai, S.; Matsumoto, K.; Sato, K.; Sasaki, S. *Angew. Chem., Int. Ed.* **2007**, *46*, 8392−8395.

(2) Namai, A.; Sakurai, S.; Nakajima, M.; Suemoto, T.; Matsumoto, K.; Goto, M.; Sasaki, S.; Ohkoshi, S.-i. *J. Am. Chem. Soc.* **2008**, *131*, 1170−1173.

(3) Watts, P. C. P.; Hsu, W. K.; Barnes, A.; Chambers, B. *Adv. Mater.* **2003**, *15*, 600−603.

(4) Shi, Z.-C.; Fan, R.-h.; Zhang, Z.-D.; Qian, L.; Gao, M.; Zhang, M.; Zheng, L.-T.; Zhang, X.-h.; Yin, L.-w. *Adv. Mater.* **2012**, *24*, 2349−2352.

(5) Liang, J.; Wang, Y.; Huang, Y.; Ma, Y.; Liu, Z.; Cai, J.; Zhang, C.; Gao, H.; Chen, Y. *Carbon* **2009**, *47*, 922−925.

(6) Li, N.; Huang, Y.; Du, F.; He, X.; Lin, X.; Gao, H.; Ma, Y.; Li, F.; Chen, Y.; Eklund, P. C. *Nano Lett.* **2006**, *6*, 1141−1145.

(7) Yang, Y.; Gupta, M. C.; Dudley, K. L.; Lawrence, R. W. *Nano Lett.* **2005**, *5*, 2131−2134.

(8) Yang, Y.; Gupta, M. C.; Dudley, K. L.; Lawrence, R. W. *Adv. Mater.* **2005**, *17*, 1999−2003.

(9) Xu, X.-B.; Li, Z.-M.; Shi, L.; Bian, X.-C.; Xiang, Z.-D. *Small* **2007**, *3*, 408−411.

(10) Ameli, A.; Jung, P. U.; Park, C. B. *Carbon* **2013**, *60*, 379−391.

(11) Geim, A. K.; MacDonald, A. H. *Phys. Today* **2007**, *60*, 35−41.

(12) Si, Y.; Samulski, E. T. *Nano Lett.* **2008**, *8*, 1679−1682.

(13) Blake, P.; Brimicombe, P. D.; Nair, R. R.; Booth, T. J.; Jiang, D.; Schedin, F.; Ponomarenko, L. A.; Morozov, S. V.; Gleeson, H. F.; Hill, E. W.; Geim, A. K.; Novoselov, K. S. *Nano Lett.* **2008**, *8*, 1704−1708.

(14) Miranda, R.; Vazquez de Parga, A. L. *Nat Nano* **2009**, *4*, 549−550.

(15) Yan, D.-X.; Ren, P.-G.; Pang, H.; Fu, Q.; Yang, M.-B.; Li, Z.-M. *J. Mater. Chem.* **2012**, *22*, 18772−18774.

(16) Zhang, H.-B.; Yan, Q.; Zheng, W.-G.; He, Z.; Yu, Z.-Z. *ACS Appl. Mater. Interfaces* **2011**, *3*, 918−924.

(17) Wang, H.; Robinson, J. T.; Diankov, G.; Dai, H. *J. Am. Chem. Soc.* **2010**, *132*, 3270−3271.

(18) Huang, X.; Li, H.; Li, S.; Wu, S.; Boey, F.; Ma, J.; Zhang, H. *Angew. Chem.* **2011**, *123*, 12453−12456.

(19) Zhang, X.-Y.; Li, H.-P.; Cui, X.-L.; Lin, Y. *J. Mater. Chem.* **2010**, *20*, 2801−2806.

(20) Xu, C.; Wang, X. *Small* **2009**, *5*, 2212−2217.

(21) Cao, X.; Shi, Y.; Shi, W.; Lu, G.; Huang, X.; Yan, Q.; Zhang, Q.; Zhang, H. *Small* **2011**, *7*, 3163−3168.

(22) Gao, L.; Ren, W.; Liu, B.; Wu, Z.-S.; Jiang, C.; Cheng, H.-M. *J. Am. Chem. Soc.* **2009**, *131*, 13934−13936.

(23) Yang, X.; Zhang, X.; Ma, Y.; Huang, Y.; Wang, Y.; Chen, Y. *J. Mater. Chem.* **2009**, *19*, 2710−2714.

(24) Cong, H.-P.; He, J.-J.; Lu, Y.; Yu, S.-H. *Small* **2010**, *6*, 169−173.

(25) Chandra, V.; Park, J.; Chun, Y.; Lee, J. W.; Hwang, I.-C.; Kim, K. S. *ACS Nano* **2010**, *4*, 3979−3986.

(26) Su, J.; Cao, M.; Ren, L.; Hu, C. *J. Phys. Chem. C* **2011**, *115*, 14469−14477.

(27) Hao, R.; Xing, R.; Xu, Z.; Hou, Y.; Gao, S.; Sun, S. *Adv. Mater.* **2010**, *22*, 2729−2742.

(28) Lu, J.; Jiao, X.; Chen, D.; Li, W. *J. Phys. Chem. C* **2009**, *113*, 4012−4017.

(29) He, H.; Gao, C. *ACS Appl. Mater. Interfaces* **2010**, *2*, 3201−3210.

(30) Sun, G.; Dong, B.; Cao, M.; Wei, B.; Hu, C. *Chem. Mater.* **2011**, *23*, 1587−1593.

(31) Guan, P. F.; Zhang, X. F.; Guo, J. J. *Appl. Phys. Lett.* **2012**, *101*, 153108.

(32) Sun, X.; He, J.; Li, G.; Tang, J.; Wang, T.; Guo, Y.; Xue, H. *J. Mater. Chem. C* **2013**, *1*, 765−777.

(33) Wang, T.; Liu, Z.; Lu, M.; Wen, B.; Ouyang, Q.; Chen, Y.; Zhu, C.; Gao, P.; Li, C.; Cao, M.; Qi, L. *J. Appl. Phys.* **2013**, *113*, 024314.

(34) Huo, X.; Liu, J.; Wang, B.; Zhang, H.; Yang, Z.; She, X.; Xi, P. *J. Mater. Chem. A* **2013**, *1*, 651−656.

(35) Miller, D.; Chatchaisucha, P.; Kumar, V. *Polymer* **2009**, *50*, 5576−5584.

(36) Miller, D.; Kumar, V. *Polymer* **2011**, *52*, 2910−2919.

(37) Zhai, W.; Yu, J.; Wu, L.; Ma, W.; He, J. *Polymer* **2006**, *47*, 7580−7589.

(38) Ling, J.; Zhai, W.; Feng, W.; Shen, B.; Zhang, J.; Zheng, W. g. *ACS Appl. Mater. Interfaces* **2013**, *5*, 2677−2684.

(39) Shen, B.; Lu, D.; Zhai, W.; Zheng, W. *J. Mater. Chem. C* **2013**, *1*, 50−53.

(40) Shen, B.; Zhai, W.; Chen, C.; Lu, D.; Wang, J.; Zheng, W. *ACS Appl. Mater. Interfaces* **2011**, *3*, 3103−3109.

(41) Shen, B.; Zhai, W.; Lu, D.; Wang, J.; Zheng, W. *RSC Adv.* **2012**, *2*, 4713−4719.

(42) Stankovich, S.; Piner, R. D.; Chen, X.; Wu, N.; Nguyen, S. T.; Ruoff, R. S. *J. Mater. Chem.* **2006**, *16*, 155−158.

(43) Zhang, H.-B.; Wang, J.-W.; Yan, Q.; Zheng, W.-G.; Chen, C.; Yu, Z.-Z. *J. Mater. Chem.* **2011**, *21*, 5392−5397.

(44) Kudin, K. N.; Ozbas, B.; Schniepp, H. C.; Prud'homme, R. K.; Aksay, I. A.; Car, R. *Nano Lett.* **2007**, *8*, 36−41.

(45) Stankovich, S.; Dikin, D. A.; Piner, R. D.; Kohlhaas, K. A.; Kleinhammes, A.; Jia, Y.; Wu, Y.; Nguyen, S. T.; Ruoff, R. S. *Carbon* **2007**, *45*, 1558−1565.

(46) Zhou, Y.; Bao, Q.; Tang, L. A. L.; Zhong, Y.; Loh, K. P. *Chem. Mater.* **2009**, *21*, 2950−2956.

(47) Paredes, J. I.; Villar-Rodil, S.; Solís-Fernández, P.; Martínez-Alonso, A.; Tascón, J. M. D. *Langmuir* **2009**, *25*, 5957−5968.

(48) Yang, D.-Q.; Rochette, J.-F.; Sacher, E. *Langmuir* **2005**, *21*, 8539−8545.

(49) Jia, B.; Gao, L.; Sun, J. *Carbon* **2007**, *45*, 1476−1481.

(50) He, F.; Fan, J.; Ma, D.; Zhang, L.; Leung, C.; Chan, H. L. *Carbon* **2010**, *48*, 3139−3144.

(51) Chae Park, H.; Po Kim, Y.; Yong Kim, H.; Soo Kang, Y. *J. Membr. Sci.* **1999**, *156*, 169−178.

(52) Li, B.-W.; Shen, Y.; Yue, Z.-X.; Nan, C.-W. *Appl. Phys. Lett.* **2006**, *89*, 132504.

(53) Das, N. C.; Liu, Y.; Yang, K.; Peng, W.; Maiti, S.; Wang, H. *Polym. Eng. Sci.* **2009**, *49*, 1627−1634.

(54) Thomassin, J.-M.; Lou, X.; Pagnoulle, C.; Saib, A.; Bednarz, L.; Huynen, I.; Jérôme, R.; Detrembleur, C. *J. Phys. Chem. C* **2007**, *111*, 11186−11192.

(55) Singh, K.; Ohlan, A.; Pham, V. H.; R, B.; Varshney, S.; Jang, J.; Hur, S. H.; Choi, W. M.; Kumar, M.; Dhawan, S. K.; Kong, B.-S.; Chung, J. S. *Nanoscale* **2013**, *5*, 2411−2420.

(56) Al-Saleh, M. H.; Sundararaj, U. *Carbon* **2009**, *47*, 1738−1746.

(57) Wang, J.; Xiang, C.; Liu, Q.; Pan, Y.; Guo, J. *Adv. Funct. Mater.* **2008**, *18*, 2995−3002.
(58) Verdejo, R.; Barroso-Bujans, F.; Rodriguez-Perez, M. A.; Antonio de Saja, J.; Lopez-Manchado, M. A. *J. Mater. Chem.* **2008**, *18*, 2221−2226.
(59) Thirumal, M.; Khastgir, D.; Singha, N. K.; Manjunath, B. S.; Naik, Y. P. *J. Appl. Polym. Sci.* **2008**, *108*, 1810−1817.
(60) Almanza, O.; Rodríguez-Pérez, M. A.; de Saja, J. A. *Polym. Int.* **2004**, *53*, 2038−2044.